CHANGE OF ULTRASONIC ATTENUATION AND MICROSTRUCTURE EVOLUTION DURING CREEP OF A STAINLESS STEEL

T.Ohtani[1], H. Ogi[2], and M. Hirao [2]
[1] Ebara Research Co., LTD., Fujisawa, Japan; [2]Osaka University, Toyonaka, Osaka, Japan

Abstract: We studied ultrasonic attenuation change during creep tests on austenitic stainless steel (JIS-SUS 316L). The material was exposed to the temperature of 973K at various stresses. We measured ultrasonic attenuation using electromagnetic acoustic resonance (EMAR), which is a contactless resonant method with the use of an EMAT and is free from extra energy losses, resulting in the measurement of intrinsic attenuation in solids. We launched polarized shear wave in the thickness direction of the plate sample to obtain the ultrasonic velocity from the resonant frequency and the attenuation coefficient from the ringdown curve at resonance. The attenuation exhibits much larger sensitivity to the damage accumulation than the velocity. Approaching the rapture, it becomes ten times as large as the initial value, which is interpreted as resulting from microstructural changes, especially, dislocation mobility. This is supported by TEM observations for dislocation structure. This technique has a potential to assess the damage advance and to predict the creep life of metals.

Introduction: Many of fossil power plants, which were constructed during 1960's and 70's and exceed more than 100,000 working hours, have presently been operating while they have underwent progressive damage, mainly from creep, as the time proceeds[1, 2]. Furthermore, by shifting the base load of power from fossil power plants to nuclear power plants, they are faced to even more severe operating condition such as daily or weekly startup and shutdown in order to correspond to rapid change of the demand. As the consequence of this trend, the material's degradation is being accelerated. Therefore, a nondestructive technique is now highly required for safely operating plants and predicting the remaining life. It is also important for the technique to be simple and quick operating to cope with the large number of measuring points.

We studied the microstructure evolution of on austenitic stainless steel (JIS-SUS 316L) during creep by monitoring ultrasonic attenuation. We applied tensile stress, ranging between 100 and 120MPa, to the material at 973K and measured ultrasonic attenuation using the electromagnetic acoustic resonance (EMAR) technique [3, 4]. EMAR is a combined technique of the resonant acoustic technique and a non-contacting electromagnetic acoustic transducer (EMAT) [4]. Incorporation of EMAT in a resonant measurement contributes to improve the weak coupling efficiency to a large extent. The attenuation measurement is inherently free from any energy loss, resulting in the pure attenuation in a metal sample. Conventional contact transducers usually cause large loss, which hinders measuring attenuation in metals. We used a bulk-wave EMAT for transmitting and receiving the polarized shear wave travelling in the thickness direction of the sample to obtain the ultrasonic velocity from the resonant frequency and then the attenuation coefficient from the ringdown curve at resonance.

Experiments: We obtained the creep specimens from hot-rolled commercial plates of on austenitic stainless steel (JIS-SUS 316L). The gauge section is 5 mm thick, 18 mm wide and 35 mm long (Fig.1). The rolling direction was parallel to the longitudinal direction of the specimen [4]. The mechanical properties at room temperature are as follows 0.2% proof stress is 261MPa, ultimate tensile strength 580MPa and elongation 59%.

We used a shear-wave EMAT of 10 x 10 mm^2 active area, which consists of an elongated-spiral coil and a pair of permanent magnets in opposite directions being normal to the specimen surface (Fig.2). The measurement principle of EMAR appears in [3].

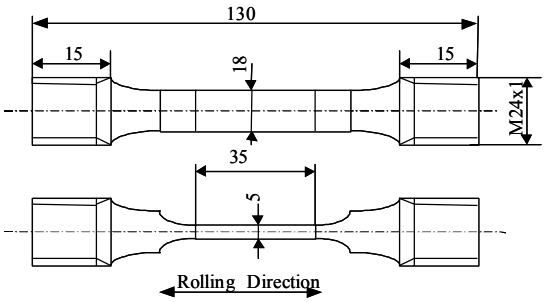

Fig.1 Specimen geometry.

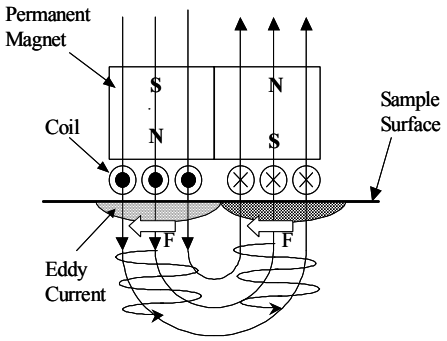

Fig.2 Structure and mechanism of shear-wave EMAT.

Creep tests were carried out at 973 K in air for three stresses of 100, 110 and 120MPa. Alongside the samples, we attached the unstressed samples to investigate only the effect of thermal history. Interrupted and Continuous tests were conducted. In Interrupted test, we interrupted creep loading and furnace-cooled the samples. After measuring the attenuation coefficients, we restarted the creep test. We repeated this procedure for every 50 or 100 hours until the rupture. In Continuous test, we continued the creep test until the creep strain reached a target value. We thus obtained a series of crept samples with various strains and measured their attenuation coefficients.

To further study the microstructure evolution as creep progress, we observed the microstructure of specimens in continuous test with optical microscope (OM), scanning electron microscope (SEM) and transmission electron microscope (TEM). TEM foils were sliced from the mid-plane at the specimen center using oil-cooling electro-discharge wire to 0.3mm thick, and then carefully polished with SiC paper to 0.2mm thick. Electrolytic polishing in 10% phosphoric acid-ethanol solution induced small center holes. Transmission electron microscopy operating at 250kV was used to obtain the micrographs at thinnest parts around holes. These micrographs are taken in the computer with the scanner for further analysis.

Results: Interrupted test: Figure 3 displays the frequency dependence of the attenuation coefficient, α, in interrupted test (973 K, 100 MPa). The time to rupture, t_r, was 1108.4 h. The polarization of the shear wave was parallel to the load. We observed that α always increases with the resonant frequency. After increasing from the start to 800 h, α decreases in the course of creep. The change only by heating is much less than those of crept samples.

Shown in Figure 4 is the relationship between α, relative velocity change $\Delta V/V_0$ (V_0: initial velocity), creep strain and life fraction, t/t_r at the 11th resonant mode under 100MPa. Rupture life was 1108.4h. α increases as the creep progress. After showing a maximum value at $t/t_r=0.6$, α quickly deceases to $t/t_r=0.9$. Afterwards, α jumps to the rupture. Whereas, $\Delta V/V_0$ slightly increases until $t/t_r=0.7$, slightly decreases until $t/t_r=0.9$ and then increases to the rupture. The maximum increment of $\Delta V/V_0$ was around 3 %. As the evolution of α and $\Delta V/V_0$ are not monotony, it is advisable to use both changes to evaluate the creep damage. Similar results were obtained at other modes and under other stresses.

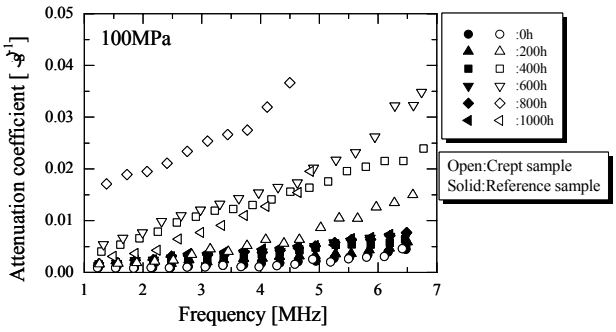

Fig.3 Frequency dependence of the shear-wave for the polarization in the stress direction (Interrupted test, 100MPa, 973K).

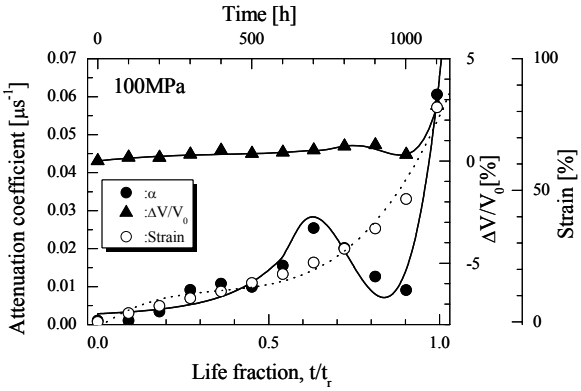

Fig.4 Attenuation and velocity evolutions of attenuation the 11th resonant mode and creep strain. The polarization is parallel to the stress direction (Interrupted test, 100MPa, 973K).

In Continuous test, we prepared nine specimens with different creep strains under 100MPa. Shown in Figure 5 is the relationship between the creep strain and creeping time. Each point is corresponding to shows each specimen. The experimental values are scattered. This figure does not show a good correlation between the creep strain and the time. That is, even though the creeping time becomes longer, the degree of creep strain does not become larger. In other word, the time can not be a reference of creep damage. Therefore, they could not apply to the remaining life prediction. Then, we estimated the creep rupture time, t_r, of each specimen from the creep curve. The estimation was made with the modified θ function [5] and a rupture parameter, P [6].

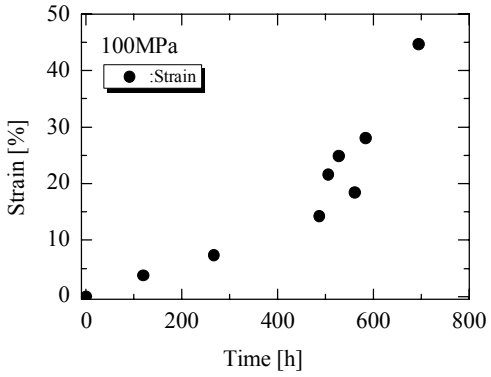

Fig. 5 The creep strains reached versus times in Continuous test (100MPa, 973K).

The relation between estimated life fraction, t/t_r, and creep strains is shown in Fig.6. Creep strains could arrange on one curve. It shows the strong correlation between the creep strain and t/t_r. Then, Figure 7 shows relationship between α, $\Delta V/V_0$, creep strain and t/t_r at the 11th resonant mode. The trend is very similar in interrupted test: that α increases and shows a peak at t/t_r=0.6. Therefore, by the observing microstructures of specimens in continuous test, we could find what influences the attenuation evolution as creep progresses.

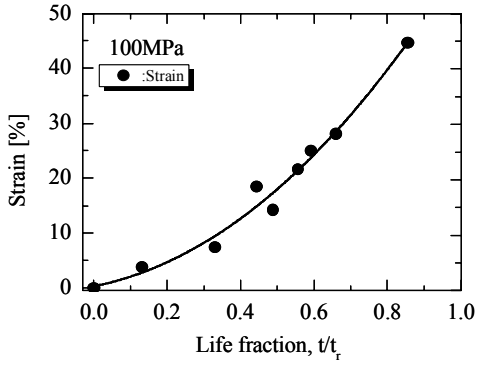

Fig.6 the creep strain reached versus estimated life fraction in Continuous test (100MPa, 973K).

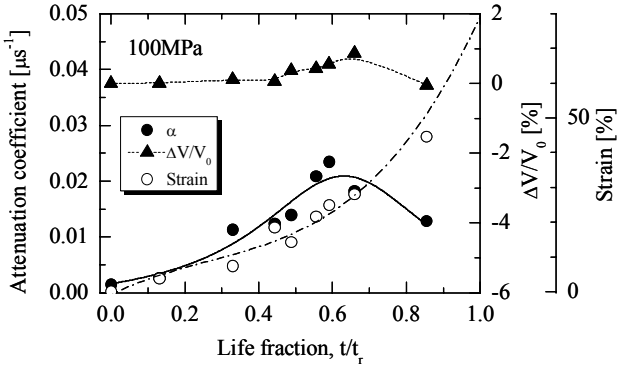

Fig.7 The relationship between α, $\Delta V/V_0$, creep strain and t/t_r at the 11th resonant mode under 100MPa in Continuous test (100MPa, 973K).

Discussion: Possible factors contributing to the change in the attenuation coefficients as creep progresses are scattering from grain boundaries, precipitations and voids, and dislocation damping for a MHz frequency range.

Grain scattering: We observed the change of average grain size as the creep progress with the optical micrographs. The average grain size remains nearly unchanged as creep progress. When the grains are much smaller than ultrasonic wavelength (>0.5mm), the attenuation caused by scattering is given by [7].

$$\alpha_s = Sd^3f^4 \quad , \tag{1}$$

where S is the scattering factor, d the average grain size, and f frequency.

We calculated α_s for the change of grain size, where $S=2.25\times10^{-10}$ $\mu sec^3/\mu m^3$ [8] which is the value of carbon steels, whose elastic moduli are similar to those of stainless steel. The change of α_s is calculated to be 2.72×10^{-3} μsec^{-1} (f=3.5MHz) and much smaller than the measurement. Moreover, nearly constant grain size can not explain the change of attenuation coefficients like in Fig. 7.

Scattering from precipitations and voids: From SEM micrographs, precipitations are observed from t/t_r=0.25. The number densities increase slightly to the rupture. Their average sizes are around 2μm. Because their sizes (>2μm) were much smaller than the probing wavelength (>0.5mm), the scattering in the Rayleigh region does occur [7];

$$\alpha_s = n\gamma/2 \sim Ca^2(ka^4), \ (ka<<1) \quad , \tag{2}$$

where n denotes the volume density of the scatter, γ is the scattering cross section, k the wave number and a the radius of the scatterer. C is constant depending on the wave mode, n, and the scatterer's type (i.e. inclusion or cavity). From SEM micrographs, we assume that the attenuation increases in a monotonous way. From Eq. (2), we calculated α_s to be less than 1% of measurement. Therefore, these effects cause only negligible changes in α and the dislocation damping can solely explain the observed acoustic response. No void was observed.

Dislocation damping: Dislocations vibrate responding to the ultrasonic stress with a phase lag because of viscosity and dissipate of the energy. This anelastic mechanism also lowers the ultrasonic velocities. The dislocation lines are pinned by point defects, precipitations and other dislocations. The pinning points act as nodes of the vibrations. From Granato and Lücke' s string model for the dislocation damping [9], we have in the lower frequency range;

$$\alpha = A_1 \Lambda L^4 f^4 \quad \text{and} \quad \Delta V/V_0 = -A_2 \Lambda L^2 \quad , \tag{3}$$

where A_1 , A_2 are positive constants depending on in shear modulus, Poisson's ratio, specific damping constant, and Burger's vector. Λ is the dislocation density and L the dislocation length. According to this model, α is proportional to Λ and the fourth power of L of the effective dislocations, which are mobile and can vibrate with the ultrasonic stress. Note that not all the dislocations interact with ultrasonics.

To a further study, we observed the evolution of dislocation structure by TEM. In the structure before the creep, dislocations distributed nearly uniform and its density was low. In the microstructure at t/t_r=0.32(Fig.7), when α increases. Many tangled dislocations were observed. The cell structures were observed. The density of pinned

dislocations became high. In the microstructure at t/t_r=0.60, when α shows a peak. Subgrains and cell structures were mixed. In the un-rearranged area, excluded in subgrains and cells, the dislocation density is higher than that at t/t_r=0.32. And then, in the microstructure at t/t_r=0.85, when α shows a minimum, the subgrains become fine and the density within subgrains reduced. The dislocation rearrangement nearly finished.

From these TEM micrographs and some quantitative results [10-12], we assumed that the change of α is related to the change of dislocation structure, especially, free dislocations in subgrains and cells because the dislocations bound in subboundaries could not vibrate responding to the ultrasonic stress. The whole phenomena can be explained as follows. The dislocation density increased from the beginning of the creep as the creep deformation advanced. After this, dislocations were tangled and the formation of cells started. By the continuous deformation, the majority of dislocations generated were spent in the formation of cells' walls or subboundaries. As a result, many subgrains developed and the dislocation density in subgrains reduced. In other area, un-rearranged one, the dislocations multiplied and the free density increased. Furthermore, by the acceleration of the rearrangement and the subgrains entirely cover the whole area. The free dislocations decreased. Finally, the crack initiated at multiplied dislocations on subgrains, grain boundaries, precipitations and the rupture started.

Conclusions: Creep damage in austenitic stainless steel (JIS-SUS 316L) at 973 K in air was evaluated through the ultrasonic attenuation measured with the Electromagnetic Acoustic Resonance (EMAR) method. Ultrasonic attenuation demonstrated a high sensitivity to the creep progress. The attenuation showed a maximum of around 60 % of the whole life, which was independent of the stress, and which was interpreted as due to the microstructure changes, especially, dislocation mobility and rearrangement. This is supported by the TEM observations. There is a clear relationship between the attenuation coefficient and the estimated life fraction, rather than the creep strain and time. Monitoring both the attenuation coefficient and velocity allows much more accurate lifetime evaluation. This technique has a potential to assess the creep damages and predict the remaining-life of metals.

References:

1. D. S. Drinon, P. K. Liaw and M. K. Rishel, (1992). *ASME PVP,* **239/MPC-33**, 5.
2. R. Viswanathan, (1989). *Damage Mechanism and Life Assessment of High Temperature Components*. ASME international.
3. M. Hirao and H. Ogi, (1989). *Ultrasonics* **35**, 413.
4. T. Ohtani, H. Ogi, H. and M. Hirao, (1999). *Rev. Prog. in QNDE*, **18**, 1847.
5. K. Maruyama, C. Harada and H. Oikawa, (1985). *J.Soc. Mater., JPN.*, **34**, 1289.
6. K. Maruyama and H. Oikawa, (1990). *Trans. ASME.J. Pressure Vessel. Technol.*, **109**, 142.
7. K. Goebbels, (1980). *Res. Tech. in NDT*, **4**, 87.
8. H. Ogi, M. Hirao and T. Honda, (1995). *J. Acoust. Soc. Am.*, **98**, 458.
9. A. Granato and K. Lücke, (1956). *J. Appl. Phys.*, **27**,789.
10. C. R. Barrett, W. D. Nix and O. D. Sherby, (1966). *Trans ASM.*, **59**, 3.
11. A. Orlova and J. Cadek, (1973). *Phil. Mag.*, **28**, 891.
12. T. Hasegawa, Y. Ikeuchi and S. Karashima, (1972). *Metal Sci. J.*, **6**, 78